Bird specimens track 135 years of atmospheric black carbon and environmental policy

Shane G. DuBay[a,b,1,2] and Carl C. Fuldner[c,1,2]

[a]Committee on Evolutionary Biology, University of Chicago, Chicago, IL 60637; [b]Life Sciences Section, Integrative Research Center, Field Museum of Natural History, Chicago, IL 60605; and [c]Department of Art History, University of Chicago, Chicago, IL 60637

Edited by Veerabhadran Ramanathan, Scripps Institution of Oceanography, University of California at San Diego, La Jolla, CA, and approved September 1, 2017 (received for review June 21, 2017)

Atmospheric black carbon has long been recognized as a public health and environmental concern. More recently, black carbon has been identified as a major, ongoing contributor to anthropogenic climate change, thus making historical emission inventories of black carbon an essential tool for assessing past climate sensitivity and modeling future climate scenarios. Current estimates of black carbon emissions for the early industrial era have high uncertainty, however, because direct environmental sampling is sparse before the mid-1950s. Using photometric reflectance data of >1,300 bird specimens drawn from natural history collections, we track relative ambient concentrations of atmospheric black carbon between 1880 and 2015 within the US Manufacturing Belt, a region historically reliant on coal and dense with industry. Our data show that black carbon levels within the region peaked during the first decade of the 20th century. Following this peak, black carbon levels were positively correlated with coal consumption through midcentury, after which they decoupled, with black carbon concentrations declining as consumption continued to rise. The precipitous drop in atmospheric black carbon at midcentury reflects policies promoting burning efficiency and fuel transitions rather than regulating emissions alone. Our findings suggest that current emission inventories based on predictive modeling underestimate levels of atmospheric black carbon for the early industrial era, suggesting that the contribution of black carbon to past climate forcing may also be underestimated. These findings build toward a spatially dynamic emission inventory of black carbon based on direct environmental sampling.

air pollution | soot | climate change | aerosols | natural history

Black carbon, the light-absorbing component of soot, is a complex carbonaceous aerosol that results from the incomplete combustion of organic matter, such as fossil fuels (1). Starting in the mid-19th century, cities within the US Manufacturing Belt—such as Chicago, Detroit, and Pittsburgh—experienced sharp rises in atmospheric soot due to their reliance on regional supplies of highly volatile soft, bituminous coal for manufacturing, domestic heating, and railway transportation (2). By the late 19th century, the palls of coal smoke hanging over industrial cities galvanized early civic reformers, who fought urban smoke pollution as an unsightly nuisance, an economic inefficiency, and a public health concern tied to respiratory illness and increased mortality (2, 3). These early, city-level efforts to mitigate atmospheric soot laid the groundwork for the modern environmental movement in the United States. While US cities no longer experience levels of atmospheric black carbon comparable to the historic peaks of the early 20th century, particle pollution remains a pressing public health and environmental issue in the United States and globally (4, 5).

Black carbon has more recently become recognized as a major contributor to anthropogenic climate change (4, 6, 7). As such, historical emission inventories are consequential for understanding black carbon's effect on past climate and accurately modeling future climate scenarios. Estimates of black carbon emissions, however, have high uncertainty for the early industrial era (1), limiting our ability to use past emissions data to extract climate sensitivity. In the United States, efforts to measure concentrations of atmospheric soot were limited to sporadic city-level surveys before the mid-1950s (8), when federal legislation targeting air pollution gave rise to a coordinated national network for atmospheric monitoring (2, 3). As a result, our current understanding of atmospheric black carbon levels before midcentury in the US Manufacturing Belt is limited to anecdotal evidence and piecemeal records. Building accurate emission inventories of climate-forcing agents like black carbon remains a key step toward establishing a more rigorous understanding of how atmospheric pollutants affect climate.

Recent efforts to estimate historical black carbon emissions have used predictive models that combine fuel consumption data with emission factors, a variable that rates the efficiency of burning technologies (9–11). Emission inventories generated by these models have been instrumental in evaluating the contribution of atmospheric black carbon to climate change (12–14), but their power is contingent on the ability of emission factors to accurately capture changes in real-world burning efficiency over time. The robustness of predictive models can be independently evaluated by direct sampling data, such as the Greenland ice-core record (15), which captures free-tropospheric emissions of black carbon from North America and stands as one of the few inventories based on a standardized, direct sampling metric of black carbon that extends back before the 1950s. The emission trends inferred from predictive models [such as

Significance

Emission inventories of major climate-forcing agents like black carbon suffer high uncertainty for the early industrial era, thereby limiting their utility for extracting past climate sensitivity to atmospheric pollutants. We identify bird specimens as incidental records of atmospheric black carbon, filling a major historical sampling gap. We find that prevailing emission inventories underestimate black carbon levels in the United States through the first decades of the 20th century, suggesting that black carbon's contribution to past climate forcing may also be underestimated. This study builds toward a robust, spatially dynamic inventory of atmospheric black carbon, highlighting the value of natural history collections as a resource for addressing present-day environmental challenges.

Author contributions: S.G.D. and C.C.F. designed research, performed research, analyzed data, and wrote the paper.

The authors declare no conflict of interest.

This article is a PNAS Direct Submission.

[1]S.G.D. and C.C.F. contributed equally to this work.

[2]To whom correspondence may be addressed. Email: dubaysg@uchicago.edu or cfuldner@uchicago.edu.

This article contains supporting information online at www.pnas.org/lookup/suppl/doi:10.1073/pnas.1710239114/-/DCSupplemental.

the Speciated Pollutant Emissions Wizard (SPEW) database from Bond et al., 2007 (11)] generally mirror the Greenland ice-core record, indicating a rise in atmospheric black carbon in the late 19th and early 20th centuries associated with increased coal consumption, with emissions dropping to near preindustrial levels shortly after midcentury. While these contrasting methods achieve comparable results, there are inconsistencies between them: The ice-core record indicates a peak in black carbon concentrations in the first decade of the 20th century, while predictive models place this peak two decades later. Reconciling this disparity not only strengthens our understanding of environmental history and policy, but also holds important consequences for downstream climate analyses.

Here, we develop an alternative direct-sampling method for estimating historical trends in atmospheric black carbon by analyzing black carbon deposition on bird specimens collected within the US Manufacturing Belt over the past 135 y. In contrast to the Greenland ice-core record, our dataset recovers historical trends in atmospheric black carbon that are geographically localized. Our method therefore bypasses assumptions about the origin of atmospheric pollutants that are necessary to interpret the ice-core samples. As a direct sampling metric, our dataset also bypasses the need to make assumptions about burning efficiency and technology shifts on which predictive models rely, providing an independent means for evaluating such models. By providing a more accurate, localized picture of historical trends in atmospheric black carbon, the results of the study yield a diverse set of implications that advance our understanding of human impacts on the physical and natural world, from assessing the impacts of black carbon on the environment to evaluating historical policies designed to clean up the air in some of the world's smokiest cities.

Results and Discussion

Black Carbon Deposition on Bird Specimens. Birds accumulate black carbon and other particulate matter on their feathers from the surrounding environment. References to plumage discoloration appear in the scientific literature as early as the 1930s, which prompted a debate over whether darkened feathers had resulted from superficial soiling or changes to internal pigmentation. The latter would indicate industrial melanism, an evolutionary phenomenon in which darker phenotypes thrive within soot-filled environments (16, 17). Using scanning electron microscopy (SEM), we confirmed that darkened breast feathers from specimens collected in the early 20th century are indeed covered in black carbon particles (Fig. 1 and Fig. S1). Given that most bird species undergo at least one annual molt to replace body feathers, black carbon deposition on specimens functions as an environmental sample from the year in which each bird was collected (we discuss the negligible effect of posthumous soiling

Fig. 1. Comparison of two Field Sparrows (*S. pusilla pusilla*), one from 1906 and one from 1996. (*Lower*) SEM micrographs of belly feathers plucked from the specimens in *Upper*. SEM micrographs of the Field Sparrow from 1906 show black carbon aggregates composed of small sphericals [a detailed description of black carbon morphology with microscopy images can be found in Bond et al., 2013 (1)]. The feather from the 1996 specimen lacks black carbon deposition. Both specimens were collected during spring months in the vicinity of Chicago. SEM images were made with a Tescan LYRA3 field emission microscope with secondary electron (SE) detection and an acceleration voltage (HV) of 3.0 kV. Feather samples were carbon-coated before imaging.

from museum storage in *SI Evidence that Bird Specimens Accumulated Black Carbon from the Environment Before Collection*).

We measured reflectance values from a time series of bird specimens that were collected within the US Manufacturing Belt between 1880 and 2015. We defined the US Manufacturing Belt as the states of Pennsylvania, Ohio, Indiana, Michigan, Illinois, and Wisconsin because these states were historically dense with industry and traditionally relied upon soft, bituminous coal, which emits greater quantities of particulate matter than the harder, anthracitic coal more prevalent in the Eastern United States (18, 19) (Fig. S2 shows localities of specimens used in study). We measured reflectance from the breast and belly feathers of each specimen. Reflectance is a photometric that describes the proportion of light reflected from a surface and is expressed as a percentage value ranging from 0% (pure black) to 100% (pure white). Black carbon, defined as the primary light-absorbing component of soot, has low reflectance properties, allowing us to quantify the relative "sootiness" of each specimen as a function of reflectance. These data establish a relative estimate of ambient concentrations of black carbon based on a standardized, direct sampling metric that extends back >70 y before continuous, multicity air-monitoring networks were in place (2, 3).

We imaged 1,347 birds from five species collected within our geographic range, comprising >95% of available specimens with adult plumage at three major natural history museums. A small number of specimens were excluded because of preparation concerns or missing collection data. Starting from a list of species that breed in the US Manufacturing Belt, we selected species that have naturally light, uniform breast and belly coloration to maximize the signal strength while allowing for comparisons across species (Fig. 1 and Fig. S3). These species included the Field Sparrow (*Spizella pusilla pusilla*), Grasshopper Sparrow (*Ammodromus savannarum pratensis*), Eastern Towhee (*Pipilo erythrophthalmus erythrophthalmus*), Horned Lark (*Eremophila alpestris pratensis*), and Red-headed Woodpecker (*Melanerpes erythrocephalus*) (Dataset S1 provides a list of vouchered specimens). Given that differences in plumage are often used to define subspecies classifications, we restricted sampling to a single subspecies per species. Each specimen was digitally photographed under standard lighting conditions, and reflectance measurements were taken from a uniform patch on the ventral side.

Each species in our sample undergoes an annual molt beginning in late summer that can last through the fall (20), which replaces soiled plumage. The absence of discoloration on freshly molted fall birds further confirmed that soot accumulation, and not industrial melanism, was primarily responsible for darkened plumage. Since molt patterns vary by individual, specimens sampled during these annual molting periods included a mix of fresh and soiled birds (Figs. S4 and S5), interfering with an accurate signal. The annual molt for each species thus had to be accounted for to recover an accurate trend in black carbon levels. We initially determined molting periods based on Pyle, 1997 (20), which we corroborated by examining monthly variances within our dataset (Fig. S4). For all species, specimens collected in the months of September–November were excluded from the final dataset; for two species, specimens from August were also removed (for more details on monthly trends, see *SI Materials and Methods* and Fig. S4). From the 1,347 specimens initially sampled, 250 fell within the defined molting periods and were excluded from final analyses, leaving 1,097 usable samples within the nonmolting monthly ranges. Historically, black carbon levels are highest during winter months (8, 15), such that the period of heaviest accumulation on feathers occurs directly after the molt. This seasonal coincidence likely obscures a monthly pattern of accumulation, but further work is needed to fully understand how birds seasonally accumulate and retain soot. Since no month-to-month trends were apparent within the designated nonmolting months, specimens were placed into groups organized by year (Fig. S4).

To integrate data across species, we normalized inverse raw reflectance values by calculating z scores within each species set. The z score for each specimen is defined as: (inverse raw reflectance value for an individual – inverse mean reflectance value for the species)/(SD of inverse reflectance for the species). Inverse reflectance was used rather than reflectance to better visualize drops in black carbon deposition, which register as an increase in reflectance and a decrease in inverse reflectance. With the normalized dataset, we estimated a trend in black carbon deposition through time using a generalized additive model (GAM) in the mgcv R package (21).

Historical Trends in Black Carbon and Environmental History. Our results show that black carbon deposition on bird specimens peaked during the first decade of the 20th century (Fig. 2). This peak is consistent with the Greenland ice-core record, anecdotal accounts, and surveys conducted in Chicago and Pittsburgh during the second decade of the 20th century, all of which indicate modest improvements in air quality after 1910 despite a steady increase in overall coal consumption (22, 23) (Fig. 2). Black carbon accumulation on specimens remained high through the 1920s. The first precipitous drop in deposition coincided with a temporary reduction in overall coal consumption during the Great Depression, which rebounded during World War II. A second and lasting drop in deposition began in the postwar period, with coal consumption declining as other fossil fuels gained traction (Fig. 2 and see Fig. S7). The second drop in black carbon deposition continues to present day, despite subsequent increases in coal consumption (Fig. 2). This sharp drop in atmospheric black carbon is consistent with the midcentury drop recovered in the Greenland ice-core record and predicted in Bond et al., 2007 (11). The Greenland ice-core record also identifies forest fires as a historical source of atmospheric black carbon, but the associated emissions were comparatively low through our study period (15), such that their influence on our trend would be minimal.

From 1880 to 1910, black carbon deposition is not strongly correlated with coal consumption (Fig. 2 and Fig. S6*A*). Our results show high black carbon levels with only a slight upward trend across these three decades, despite a sharp increase in coal consumption over the same period (Fig. 2). While ambient concentrations of black carbon hit a historical peak in this period, the relatively constant levels of black carbon on specimens suggest that period reforms and antismoke initiatives registered a modest mitigating effect, reducing the growth in black carbon levels relative to consumption. Toward the end of the 19th century, civic reformers organized to combat urban smoke pollution (2, 3). In 1881, Chicago and Cincinnati passed the first municipal smoke ordinances in the United States. These laws focused on regulating emissions, but they exempted residential burning and proved difficult to enforce (2). By 1910, most cities in the US Manufacturing Belt had established municipal departments specifically devoted to smoke abatement (3), and reform efforts began to expand beyond litigation to encompass education and technology-based solutions (24).

From 1910 to 1960, black carbon deposition was positively correlated with trends in coal consumption (Fig. 2 and Fig. S6*B*). During this period, reform efforts focused on curbing emissions through education and by promoting technologies to burn coal more efficiently. Despite these concerted efforts to rein in soot emissions, our data confirm that the overall concentration of atmospheric black carbon remained tied to coal consumption through midcentury (Fig. 2). Our results suggest that efforts to regulate emissions directly were largely ineffective at reducing overall levels of atmospheric black carbon.

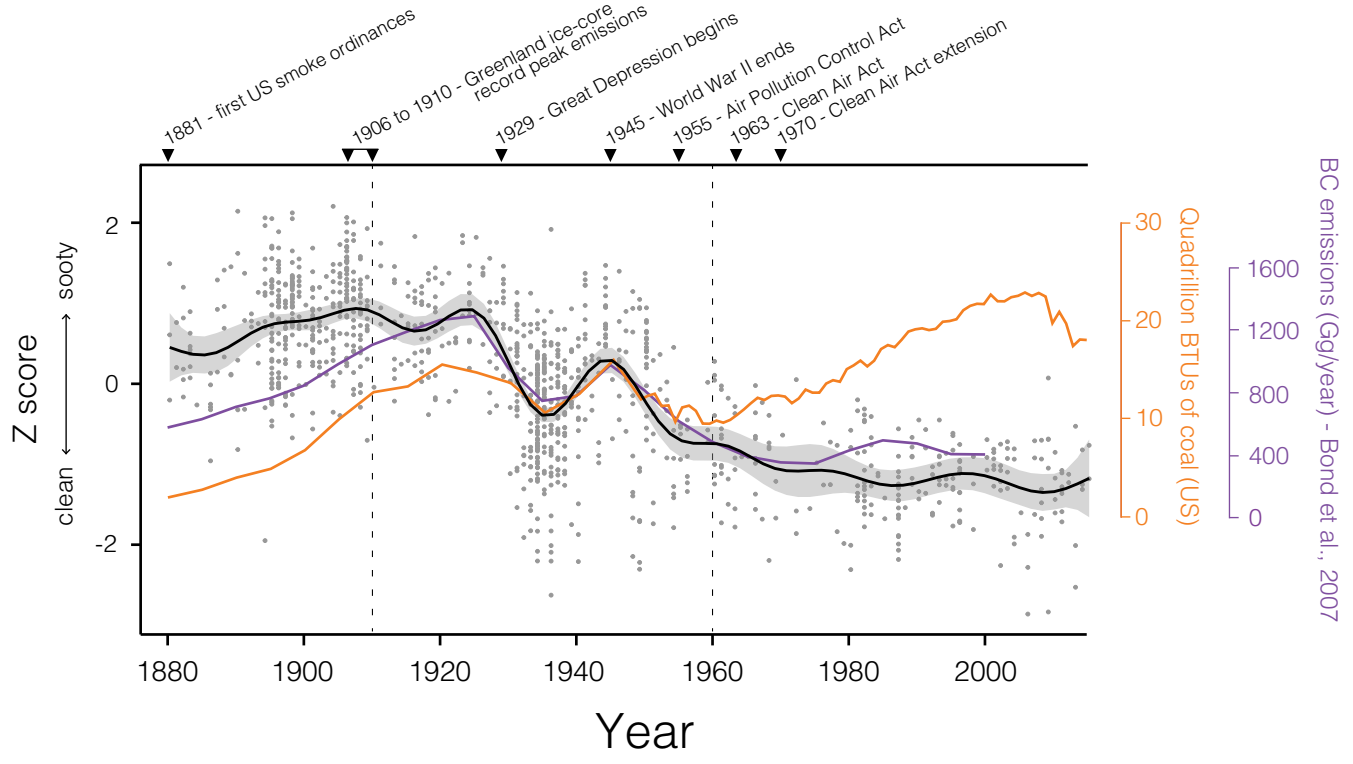

Fig. 2. Black carbon deposition on specimens of five bird species from the US Manufacturing Belt, collected between 1880 and 2015. Each point represents the z score for an individual specimen ($n = 1,097$) based on the inverse raw reflectance value taken from its breast and belly feathers. The black line is a GAM ($k = 20$) with 95% confidence limits (indicated by the shaded area), determined from the individual specimens (details on how k was determined can be found in *SI Materials and Methods* and Fig. S10. Fig. S13 shows species-specific trends). The orange line is consumption for coal in the United States expressed in British thermal units (BTUs) (US Energy Information Administration). Before 1950, coal consumption data are available in 5-y intervals. After 1950, coal consumption data are yearly. The purple line shows estimates of total US black carbon (BC) emissions from Bond et al., 2007 (11), which uses fuel consumption data and emission factor data to generate a historical emission inventory. The dashed line at 1910 denotes the progressive shift in cities within the US Manufacturing Belt from prosecuting to educating emissions violators. The dashed line at 1960 denotes the approximate moment after which black carbon emissions become decoupled from coal consumption.

During the second half of the 20th century, black carbon deposition on specimens became decoupled from coal consumption (Fig. 2 and Fig. S6*C*). As consumption began to rise again in the postwar period, atmospheric black carbon continued to decline. This decoupling can be explained by a new approach to city-level legislation, which targeted the types of fuel consumed in both domestic and industrial sectors rather than regulating emissions directly. New regulations addressed the distribution of bituminous coal and mandated that consumers of soft coals use mechanical stokers or switch to smokeless fuels (2). These reforms effectively eliminated bituminous coal as a fuel source from residential furnaces, which are estimated to have produced over half of black carbon emissions during the early 20th century (9). The success of these new regulations was contingent upon providing economically viable fuel alternatives. Following a successful model implemented in St. Louis in 1940, Pittsburgh began subsidizing harder, low-volatile coal for domestic use in 1946 (22). St. Louis had seen the benefits of this new approach almost immediately, experiencing an 83.5% decrease in the total hours of thick atmospheric soot during the winter of 1940–41 (25). Following WWII, US cities also began transitioning to alternative fuel sources, specifically petroleum and natural gas (Fig. S7). By 1950, 66% of households in Pittsburgh were heated with natural gas, up from 17% a decade earlier (26). Around the same time, electricity production in the United States shifted away from scattered, coal-powered steam boilers to centralized power plants (27). While these plants were more efficient, they drove the steady rise in coal consumption in the second half of the 20th century as they met the increasing demands for electricity. Together, the increased availability of fuel alternatives and the centralization of power production account for the decoupling of coal consumption from black carbon deposition on specimens. While soot mitigation in the United States took decades to achieve, the solutions proved to be relatively straightforward: Regulate the types of fuel consumed and promote affordable alternative fuel options.

With black carbon levels declining by midcentury (Fig. 2), the United States entered a new era of air pollution and environmental policy. Decades of research and activism aimed at mitigating soot pollution culminated in the passage of the Air Pollution Control Act of 1955, the first federal air pollution legislation in the United States. This act did not regulate or control pollution levels, but directed money toward research into air pollution, helping to establish a coordinated, national network to monitor air quality. In 1963, the first incarnation of the Clean Air Act established federal limits on a variety of atmospheric pollutants, but by then, high levels of atmospheric black carbon had already receded (Fig. 2).

Black Carbon Levels Exceed Predictive Model Estimates. Our results suggest that black carbon levels were higher at the start of the 20th century than estimates generated from predictive models (9, 11). While Bond et al., 2007 (11) considered black carbon emissions on a national scale, our studies are largely comparable since their estimates for the United States are driven by bituminous coal, which was disproportionately consumed within the

Manufacturing Belt (2, 19). Between 1880 and 1910, we recovered black carbon levels that were higher than the one estimated by Bond et al., 2007 (11) (Fig. 2 and Fig. S8*A*), a finding corroborated by the Greenland ice-core record. Our results are consistent with the peak concentrations in the ice-core record during the first decade of the 20th century, but we recovered higher relative concentrations between 1880 and 1900. This discrepancy could be explained if certain types of particles precipitated from the atmosphere before reaching Greenland.

The lower estimates recovered by Bond et al., 2007 (11) are likely explained by the lack of reliable emissions data from the early industrial period used to parameterize predictive models. As Bond et al., 2007 (11) acknowledge, this lack of data introduces high uncertainty into their model. Additionally, inconsistent burning practices and technology shifts across and within emitting sectors are difficult to account for in emission factors. Bond et al., 2007 (11) assumes that the burning efficiency for a given technology remains constant, without accounting for incremental improvements in operating procedures through time. Operating efficiency became a key target of reform and education efforts after 1910, and our data suggest that these efforts did in fact register a modest mitigating effect. Emission factors in predictive models are thus limited in their ability to reflect real-world burning efficiency because of the inherent difficulties in quantifying variables like operating efficiency and asymmetric technology shifts throughout a given region or sector. Since our measurements are based on direct sampling of ambient concentrations, we are able to bypass assumptions about efficiency and technology implementation. However, translation of our measurements to emissions is not straightforward since, as with the ice-core record, the relationship between ambient concentrations and emissions depends on meteorological factors, which may have changed over time.

While our results show that current predictive models likely underestimate levels of atmospheric black carbon for the early industrial era, as consumption and emission factor data become more reliable through the 20th century, our results are positively correlated with predictive models (Fig. 2 and Fig. S8*B*). After 1910, we recovered a trend in atmospheric black carbon that is strikingly consistent with the trend produced by Bond et al., 2007 (11) (Fig. 2 and Fig. S8*B*). This result suggests that predictive models effectively recover emissions when sufficient data exist to parameterize the model. Our study thus provides support for the power of predictive modeling methods, while also indicating that black carbon emissions in the United States at the outset of the 20th century were higher than current estimates. This finding suggests that the climate-forcing effects of black carbon may also be underestimated for this period.

Building a Usable Emission Inventory. A limitation of our current method is that reflectance values from specimens track relative trends in black carbon concentrations rather than recovering mass concentrations of atmospheric black carbon. Calibrating reflectance to a standard unit of mass concentration represents a next step toward building a usable, spatially dynamic emission inventory. Black carbon levels in Asian cities like Beijing and Delhi resemble those of the US Manufacturing Belt of a century ago (11), and we now have precise methods for measuring black carbon mass concentrations. By comparing contemporaneous measurements taken from these Asian cities with specimens collected from the same locations, our pre-1950 reflectance values could be calibrated to derive historical mass concentrations of black carbon from our sample. Once mass concentrations have been established, it would then become possible to estimate overall emissions for the region, although this step introduces additional challenges. Ambient concentrations and emissions are related yet distinct measures, and the translation between the two requires consideration of local topography and meteorology.

Additional insights are discoverable through a more thorough material analysis of black carbon on birds. The size and shape of black carbon particles and aggregates define their optical properties and climate-forcing effects (1, 28), and thus knowing the historical size distribution of black carbon particles is critical for evaluating their climate impacts and building a usable emission inventory. Robust datasets of size distribution of black carbon particles, however, are similarly lacking before the 1950s, and these data are likewise difficult to predict with any certainty because particle size is dependent on a number of interacting variables, including the chemical composition of the fuel source, along with the technology and operating procedures used to burn the fuel. By analyzing black carbon deposits on bird specimens for their physical properties, the size distribution from the early industrial era could be directly estimated for a given year and locale. These data would be invaluable for developing more robust emission inventories of atmospheric black carbon.

Conclusions

This research highlights the unexpected ways in which museum materials can yield insights about the physical and natural world and help address present-day environmental challenges. Natural history collections are powerful resources for tracking environmental pollutants through time (29, 30) because specimens provide durable snapshots of the past environments from which they were drawn. For this study, bird specimens provided an incidental record of atmospheric black carbon from a period before standardized methods and coordinated systems for assessing air quality were in place. We focused on the US Manufacturing Belt because of its historical importance as a polluting region, but our dataset can naturally be expanded to encompass other regions with long industrial histories, such as Western Europe. Natural history collections thus represent a unique resource for exploring past environments and environmental history.

For the purpose of this study, we used bird specimens as a direct sampling metric to assess historical concentrations of black carbon, which we used in turn to evaluate past environmental policy. Our study, however, also highlights the impact of environmental pollution on wildlife. Our samples show that black carbon particulate covered the landscape along with its living inhabitants. Black carbon accumulation on birds has potential implications for evolutionary pathways because plumage is fundamental in avian displays and signaling. Birds use their plumage to attract mates, defend territories, and/or camouflage themselves within the landscape to escape detection from predators. What happens when bright, sexually selected plumage patches are coated in soot, obscuring plumage signals that have evolved over hundreds of thousands of years? What are the consequences of black carbon deposition for visual predators when animal prey coloration is homogenized with the surrounding environment? How black carbon deposition on feathers has impacted signaling within and among species remains an open question.

Materials and Methods

Reflectance has long been used as an efficient and reliable metric in atmospheric sampling (31). For the purposes of this study, we were interested in deriving relative ambient concentrations from black carbon deposition on bird feathers. Since black carbon is defined by its light-absorbing properties, trends of black carbon deposition on specimens can be quantified as a function of the reduction in reflectance relative to unsoiled specimens. We adapted photography methods from Stevens et al., 2007, and McKay, 2013 (32, 33) to quantify the reflectance of each specimen. For complete details of the materials and methods used to photograph specimens, see *SI Materials and Methods*.

To determine the reflectance value for each specimen from a digital image, we used regression equations calculated from reflectance standards to convert raw sensor data to known reflectance values. We calculated R, G, and B channel-specific regressions from Munsell Neutral Value Scale reflectance standards in RawDigger (Version 1.2.11) for each of our three

shooting locations: The Field Museum, Chicago; University of Michigan Museum of Zoology, Ann Arbor; and Carnegie Museum of Natural History, Pittsburgh (Fig. S9). Since our camera's CMOS sensor incorporates an additional G channel (G2), we averaged both G-channel values to produce a single G-channel regression. The equations for each regression line can be found in Fig. S9. We uploaded the digital photograph of each specimen into RawDigger and sampled the uniform white patch on the ventral side of each specimen. We recovered median raw R, G/G2, and B channel sensor values from a sampling area that ranged from 25 to 900 mm^2. Since feathers are a textured, heterogeneous surface, median values were used to minimize any effect of outliers. For each specimen, the sample area was determined by selecting a large continuous area without conspicuous portions of exposed skin, staining due to residual fat deposits, or other preparation and conservation issues (see Dataset S1 for sample areas). We used the collection-specific regression equations to calculate reflectance values separately for R, G/G2, and B channels for each specimen. We then averaged the three channel-specific reflectance values to obtain a composite reflectance value for each specimen.

ACKNOWLEDGMENTS. We thank contributors past and present to natural history collections. Projects like this would not be possible without the commitment of individuals to collections, specifically: David Willard, Ben Marks, Sushma Reddy, Josh Engel, Shannon Hackett, and John Bates at The Field Museum; Janet Hinshaw and Benjamin Winger at the University of Michigan Museum of Zoology; and Steve Rogers at the Carnegie Museum of Natural History. David Willard and John Bates first introduced us to "sooty" birds in collections. We thank Julie Marie Lemon, Marissa Lee Benedict, and the Arts, Science + Culture Initiative at the University of Chicago, which funded this project. We thank Philipp Heck and Levke Kööp for help with SEM imaging; Iliah Borg for help with RawDigger software; the Statistics Consulting Program at the University of Chicago for advice with analyses; and Bret Hoffman for help with Fig. S3. We thank Hussein Al-Asadi, John Bates, Jonah Bloch-Johnson, João Capurucho, Jacob Cooper, Nick Crouch, Chad Eliason, Ryan Fuller, Shannon Hackett, Daniel Hooper, David Jablonski, Yanzhu Ji, Dallas Krentzel, Elizabeth Moyer, Amy Owen, Daniela Palmer, John Park, Trevor Price, Heather Skeen, Joel Snyder, Tim Sosa, K. Supriya, Alex White, and two anonymous reviewers for thoughtful comments that improved this manuscript.

1. Bond TC, et al. (2013) Bounding the role of black carbon in the climate system: A scientific assessment. *J Geophys Res Atmos* 118:5380–5552.
2. Stradling D (1999) *Smokestacks and Progressives: Environmentalists, Engineers and Air Quality in America, 1881–1951* (Johns Hopkins Univ Press, Baltimore).
3. Stern AC, Professor E (1982) History of air pollution legislation in the United States. *J Air Pollut Control Assoc* 32:44–61.
4. Ramanathan V, Carmichael G (2008) Global and regional climate changes due to black carbon. *Nat Geosci* 1:221–227.
5. Shindell D, et al. (2012) Simultaneously mitigating near-term climate change and improving human health and food security. *Science* 335:183–189.
6. Hansen J, Sato M, Ruedy R, Lacis A, Oinas V (2000) Global warming in the twenty-first century: An alternative scenario. *Proc Natl Acad Sci USA* 97:9875–9880.
7. Jacobson MZ (2000) Physically-based treatment of elemental carbon optics: Implications for global direct forcing of aerosols. *Geophys Res Lett* 27:217–220.
8. Ives JE, et al. (1936) *Atmospheric Pollution of American Cities for the Years 1931 to 1933 with Special Reference to the Solid Constituents of the Pollution* (US Government Printing Office, Washington, DC).
9. Novakov T, et al. (2003) Large historical changes of fossil-fuel black carbon aerosols. *Geophys Res Lett* 30:1324.
10. Ito A, Penner JE (2005) Historical emissions of carbonaceous aerosols from biomass and fossil fuel burning for the period 1870–2000. *Glob Biogeochem Cycles* 19:1–14.
11. Bond TC, et al. (2007) Historical emissions of black and organic carbon aerosol from energy-related combustion, 1850–2000. *Glob Biogeochem Cycles* 21:GB2018.
12. Jacobson MZ (2004) Climate response of fossil fuel and biofuel soot, accounting for soot's feedback to snow and sea ice albedo and emissivity. *J Geophys Res Atmospheres* 109:D21201.
13. Hansen J, et al. (2005) Efficacy of climate forcings. *J Geophys Res Atmospheres* 110:D18104.
14. Shindell D, Faluvegi G (2009) Climate response to regional radiative forcing during the twentieth century. *Nat Geosci* 2:294–300.
15. McConnell JR, et al. (2007) 20th-century industrial black carbon emissions altered arctic climate forcing. *Science* 317:1381–1384.
16. Hardy E (1937) Polluted wild life. *Country Life* 81:676.
17. Harrison C (1963) 'Industrial' discoloration of house sparrows and other birds. *Br Birds* 56:296–297.
18. Hartshorne R (1936) A new map of the manufacturing belt of North America. *Econ Geogr* 12:45–53.
19. Bond TC, et al. (2004) A technology-based global inventory of black and organic carbon emissions from combustion. *J Geophys Res Atmospheres* 109.
20. Pyle P (1997) *Identification Guide to North American Birds: Columbidae to Ploceidae* (Slate Creek Press, Point Reyes Station, CA).
21. Wood S (2011) Fast stable restricted maximum likelihood and marginal likelihood estimation of semiparametric generalized linear models. *J Roy Stat Soc Stat Meth* 73:3–36.
22. Davidson CI (1979) Air pollution in Pittsburgh: A historical perspective. *J Air Pollut Control Assoc* 29:1035–1041.
23. Bachmann J (2007) Will the circle be unbroken: A history of the U.S. National ambient air quality standards. *J Air Waste Manag Assoc* 57:652–697.
24. Grinder RD (1980) The battle for clean air: The smoke problem in post-civil war America. *Pollution and Reform in American Cities, 1870–1930* (Univ of Texas Press, Austin).
25. Tarr JA, Zimring C (1997) *The Struggle for Smoke Control in St. Louis. Common Fields: An Environmental History of St. Louis* (Missouri HIstorical Society Press, St. Louis), pp 199–220.
26. Tarr JA (1981) Changing fuel use behavior: The Pittsburgh smoke control movement, 1940–1950. *Technol Forecast Social Change* 20:331–346.
27. Platt HL (1991) *The Electric City: Energy and the Growth of the Chicago Area, 1880–1930* (Univ of Chicago Press, Chicago).
28. Koch D, et al. (2009) Evaluation of black carbon estimations in global aerosol models. *Atmos Chem Phys* 9:9001–9026.
29. Hickey JJ, Anderson DW (1968) Chlorinated hydrocarbons and egg shell changes in raptorial and fish-eating birds. *Science* 162:271–273.
30. Thompson DR, Furness RW, Monteiro LR (1998) Seabirds as biomonitors of mercury inputs to epipelagic and mesopelagic marine food chains. *Sci Total Environ* 213:299–305.
31. Penner JE, Novakov T (1996) Carbonaceous particles in the atmosphere: A historical perspective to the fifth international conference on carbonaceous particles in the atmosphere. *J Geophys Res Atmos* 101:19373–19378.
32. Stevens M, PARraga CA, Cuthill IC, Partridge JC, Troscianko TS (2007) Using digital photography to study animal coloration. *Biol J Linn Soc* 90:211–237.
33. McKay BD (2013) The use of digital photography in systematics. *Biol J Linn Soc* 110: 1–13.
34. Westland S, Ripamonti C, Cheung V (2012) *Computational Colour Science Using MATLAB* (John Wiley & Sons, Chichester, UK).
35. Peng RD, Dominici F, Louis TA (2006) Model choice in time series studies of air pollution and mortality. *J Roy Stat Soc Stat Soc* 169:179–203.
36. Chuang YH, et al. (2011) Generalized linear mixed models in time series studies of air pollution. *Atmos Pollut Res* 2:428–435.

Supporting Information

DuBay and Fuldner 10.1073/pnas.1710239114

SI Materials and Methods

Photographing Specimens. Specimens were imaged with a mirrorless interchangeable lens camera (Sony a7R II) paired with a native 55 mm lens (Sonnar T* FE 55 mm F1.8 ZA), positioned at a fixed height of 72 cm over a self-contained light box (MK Digital Direct Photo-e-Box BIO) outfitted with 28-W continuous full-spectrum fluorescent bulbs (6,500 K, 84CRI) run through 120-V AC 60-Hz electronic ballasts. Specimens were illuminated by using top, side, and back bulbs in the light box, omitting the bottom (stage) bulbs and supplemental LED bulbs to ensure an even distribution of diffuse light from a single illuminant type source. At the beginning of each imaging session, the lighting elements were turned on and allowed to warm up for 20 min before shooting. Specimens were oriented so that the target area on the breast was positioned at the center of the camera's field of view. The light box was fully enclosed during each exposure, except for a rectangular aperture on the top, sized to fit the camera's field of view. Overhead lighting was turned off in each of the shooting locations, and windows were covered to further reduce ambient light leakage.

The images were captured in 14-bit uncompressed raw format and analyzed by using RawDigger software (Version 1.2.11), which provides access to raw data directly recorded by the digital camera's CMOS sensor. Analyzing the raw sensor data directly enabled us to bypass the linearization step described by Stevens et al., 2007, and McKay, 2013 (32, 33), since the raw values have not been altered by nonlinear gamma encoding algorithms that are introduced when raw sensor data are converted into conventional image formats, such as JPEG or TIFF (34). Before shooting, we tested the linearity of the camera's CMOS sensor following the procedure outlined in Stevens et al., 2007 (32) and we found that the sensor provided a linear response over the entire dynamic range (Fig. S9).

Exposure settings (shutter speed, aperture, and ISO) were optimized through a series of trials using reflectance standards. We conducted trials using four types of reflectance standards, including the XRite ColorChecker Passport (8-step), QPcard 101 (3-step), Labsphere Spectralon Diffuse Reflectance Standards (10 reference targets), and Munsell Neutral Value Scale matte finish (31-step). We found that each standard provided comparable results, but we selected the Munsell Neutral Value Scale as our primary standards because it was relatively affordable, provided the largest number of reference points, and included published reflectance percentages printed directly on the cards for easy reference. To determine exposure settings, we analyzed trial images in RawDigger with a goal of maximizing the dynamic range (defined as the distance between minimum and maximum light intensities) without introducing signal clipping on any of the color channels (R-G-B-G2), which occurs when certain clusters of pixels fall outside of the dynamic range due to overexposure (saturation). It is essential to refer to the raw data when assessing whether signal clipping has occurred, since the channel-specific histograms on many digital cameras' displays incorporate gamma-encoding algorithms that make it difficult to tell whether signal clipping has actually occurred. Exposure settings maximizing dynamic range will often indicate overexposed areas on the camera's built-in displays, when no signal clipping in the raw file has taken place.

The ISO was set to 100 to ensure a limited amount of digital noise. Based on the trials, an aperture of f/16 was chosen to minimize optical vignetting (light falloff), which is introduced at lower focal ratios, while providing a depth of field that would ensure that the target area appeared in focus for all specimens, which varied in height due to differences in natural size and preparation of the specimens. With these parameters in place, a shutter speed of 1/25 s was selected to maximize the dynamic range.

While the use of a light box ensured relatively even and continuous illumination compared with open studio lighting arrangements, perfectly consistent illumination is difficult to achieve in practice. Some unevenness was discovered in blank reference images, which was determined to have resulted from lens variables (optical vignetting and lens flare) and may have also been influenced by the arrangement of the bulbs in the light box. To account for these factors, the target area for each specimen was confined to a 3- $\times$ 3-inch square, which limited variance in illumination to $<1\%$.

Under the constant lighting conditions that a light box provides, reflectance standards theoretically only need to be photographed once over the course of shooting to generate calibration regressions. In practice, however, some minor variations in overall illumination were discovered between the three locations, which may have been due to light leakage or slight variations in the voltage supply to the bulbs at each location. This variation, however, was easily accounted for by imaging the Munsell Neutral Value Scale reflectance standards at each location and calculating reflectance values for specimens with location-specific reflectance regressions. Since reflectance is expressed as a percentage, and these percentage values are relative to the standards, no additional adjustments were needed to normalize the color channels or calibrate the values across shooting locations. We photographed each card of the Munsell Neutral Value separately at The Field Museum and Carnegie Museum of Natural History, positioning each card at the center of the field of view in the same area where we measured reflectance from bird feathers. To determine reflectance regressions from these locations, we used all 31 reflectance standards (ranging from 3.1 to 90% reflectance). At the University of Michigan Museum of Zoology, we photographed the Munsell Neutral Value Scale fanned out in single photograph. For this sample, we only included 12 reflectance steps (ranging from 9 to 84.2% reflectance) that fell within the target area (Fig. S9).

Determining the Smoothing Function for the GAM. Smoothing parameters for GAMs can be determined in mgcv by using functions such as GCV that minimize residual deviance (goodness of fit) and degrees of freedom (21). With our final dataset, the GAM estimated a smoothing function of $k = 10$ (this model is plotted in Fig. S10), which recovered a smoother curve than $k = 20$ (Fig. 2). Oversmoothing, however, can obscure signals in the data (35, 36), which appears to be happening with $k = 10$ based on our knowledge of likely inflection points (such as the 1929 US stock market crash) that are present in the consumption data and the Greenland ice-core record. For reference, in Fig. S10, we include a variety of smoothing functions from $k = 10$ to $k = 100$. Based on the comparison of possible k values, $k = 10$ appears to apply an overly powerful smoothing operation in the GAM, forcing the first decline of black carbon to begin in the early 1920s rather than the end of the decade where we would expect it to appear based on consumption trends; $k = 13$ through $k = 35$ recovers trends that are effectively identical, which appears to recover important signals in the data that over smoothing misses; $k = 36$ and greater generate toothy trends that overrepresent random variations within the sample set. Based on the variation in the shape of different GAMs, we selected a smoothing

function of $k = 20$ to produce a relatively smooth trend line that still maintained a distinctive shape that allowed for comparison against consumption data.

How Sampling Months Were Determined. Beginning in late summer, each species used in the study initiates an annual molt to replace worn and soiled body feathers with fresh plumage. This molting period can last through the fall months (20). Natural variation in the timing of the molt produces a mix of birds with fresh and soiled plumage among specimens sampled from these months. This annual molt signal was apparent in our sample, with samples from fall months producing shifts in mean reflectance caused by the introduction of freshly molted birds, along with uncharacteristically broad ranges in reflectance values compared with other months (Figs. S4 and S5). Freshly molted individuals do not provide evidence for atmospheric conditions in a given year, warranting their removal from the final dataset. Since freshly molted birds begin to accumulate particulate matter immediately after the molting cycle is complete, rather than selectively evaluating which individuals had recently molted, all of the specimens sampled during these months were removed. We determined the months to exclude for each species based on abrupt shifts in mean reflectance between months, which are indicative of annual molting patterns. For example, in Horned Larks, reflectance values shift abruptly between July and August and then increase again between November and December, indicating that the sample of birds in the months of August–November includes a substantial number freshly molted individuals (Fig. S4). Following this method, the months of August–November were excluded for Horned Larks and Red-headed Woodpeckers, and the months of September–November were excluded for Field Sparrows, Grasshopper Sparrows, and Eastern Towhees (Fig. S4). We could be confident in these shifts given their seasonal timing, since overall black carbon emissions seasonally trend in the opposite direction for a given year in the Northern Hemisphere, as fuel consumption increases to meet heating needs when average temperatures drop (8, 15). We limited this inquiry to the years 1880–1950 because after midcentury, birds are substantially cleaner in all months, compromising our ability to detect monthly breakpoints.

SI Evidence that Bird Specimens Accumulated Black Carbon from the Environment Before Collection

To link reflectance data to black carbon levels for a single year, it had to be established that black carbon accumulation occurred before collection. Multiple lines of evidence indicated that the black carbon accumulated on bird specimens originated from the environment while the birds were alive and not from posthumous soiling or discoloration that occurred while being stored in a collection:

(1) Since posthumous soiling would accrete continuously, if soiling had occurred over time in storage, it would not have been possible to observe seasonal differences, and any monthly trends that result from the annual molting cycle would have been erased or vastly diminished, particularly in older specimens. We found that consistent numbers of birds collected during the fall were much cleaner in a given year, indicating freshly molted individuals (Figs. S4 and S5). These patterns were observable even among birds that had been in the same collections as soiled birds, stored together since the time of collection.

(2) We conducted a visual survey of bird specimens collected outside the US Manufacturing Belt from other parts of the United States or from less industrialized countries during our 135-y sampling period. If posthumous soiling had occurred within our sample, we would have expected specimens collected in these nonindustrialized regions to have exhibited comparable levels of soiling to those in our sample, which we did not find. A visual example of this evidence can be seen in Fig. S11, which shows five Horned Larks collected in Illinois and five Horned Larks collected along the western coast of North America. All 10 birds were collected during nonmolting months between 1903 and 1922, a period in which consistently high levels of black carbon deposition were found on bird specimens collected within the US Manufacturing Belt.

(3) If specimens in our sample accumulated black carbon from sitting in museum collections, we would have expected specimens to have soiled ventral sides and cleaner dorsal sides because they generally rest in drawers with their breast and belly facing up. The dorsal side of the specimens would thus have been protected from soot precipitate. We found, however, that both sides of specimens exhibited soiling (Fig. S12).

(4) If substantial posthumous soiling had occurred within our samples, we would have predicted that the oldest specimens would have been the sootiest based on gradual accumulation over time. However, we found a slight increasing trend in black carbon deposition between 1880 and 1910.

Together, these lines of evidence suggest that any posthumous soiling from sitting in museum storage is negligible.

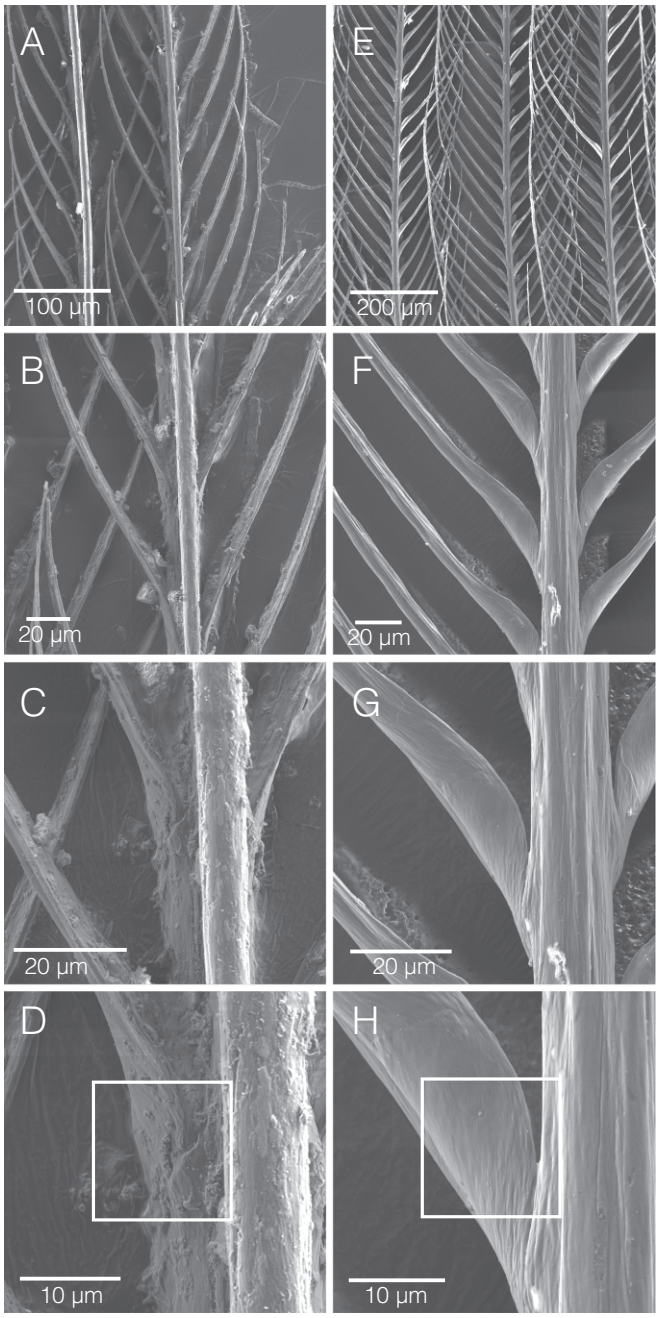

Fig. S1. Additional SEM micrographs, taken at different magnifications, from the Field Sparrows (*S. pusilla pusilla*) in Fig. 1. *A–D* are from the soiled 1906 specimen. *E–H* are from the clean 1996 specimen. The micrographs for each specimen are progressively higher in magnification. The white boxes in *D* and *H* outline the areas shown in Fig. 1.

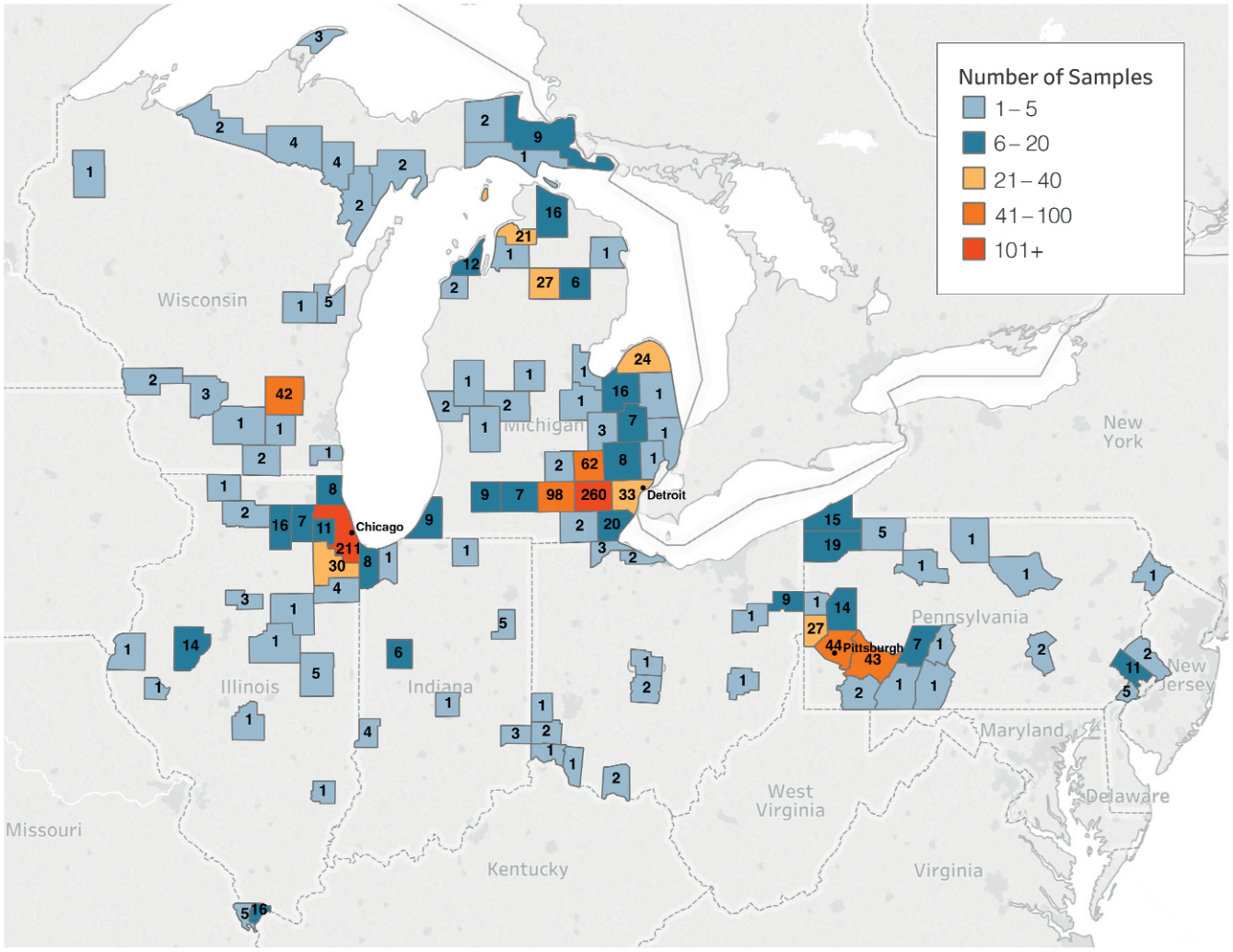

Fig. S2. Map showing the collection localities for 1,345 of 1,347 specimens used in this study. The remaining two specimens lack county locality data. Counties are shaded based on the density of sampling within the county. The number of specimens from each county is printed within each county.

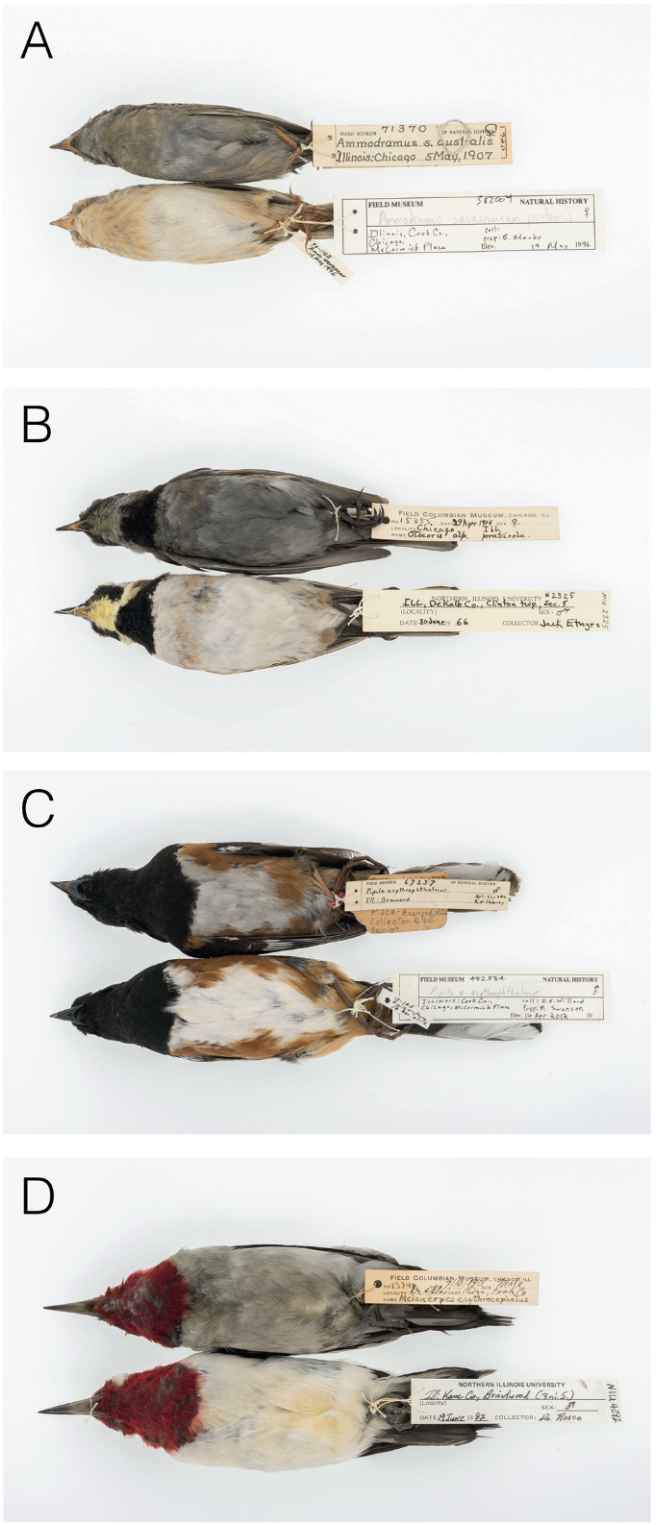

Fig. S3. Comparisons of old and young specimens for the four species pairs not shown in Fig. 2. (*A*) Grasshopper Sparrows (*A. savannarum pratensis*) from 1907 (*Upper*) and 1996 (*Lower*). (*B*) Horned Larks (*E. alpestris pratensis*) from 1904 (*Upper*) and 1966 (*Lower*). (*C*) Eastern Towhees (*P. erythrophthalmus erythrophthalmus*) from 1906 (*Upper*) and 2012 (*Lower*). (*D*) Red-headed Woodpeckers (*M. erythrocephalus*) from 1901 (*Upper*) and 1982 (*Lower*).

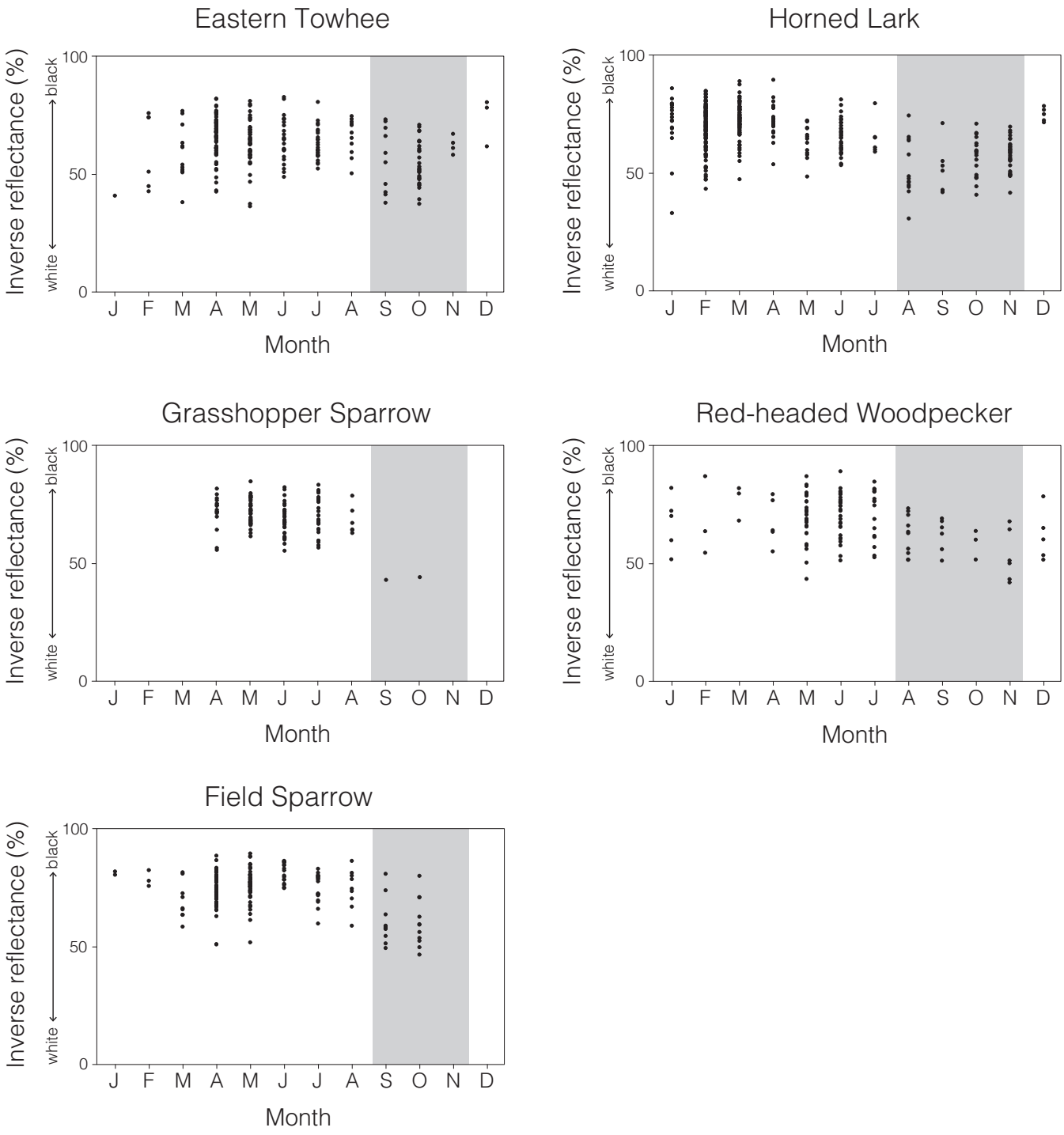

Fig. S4. Monthly trends in black carbon deposition for each species before 1950. Inverse reflectance is reported rather than reflectance to express drops in black carbon emissions, which register as increased reflectance values. The shaded areas are the months excluded from final analyses for each species, which are applied to all years. Sampling is sparse for Grasshopper Sparrows and Field Sparrows in the US Manufacturing Belt during fall and winter months because these species predominately migrate out of the region.

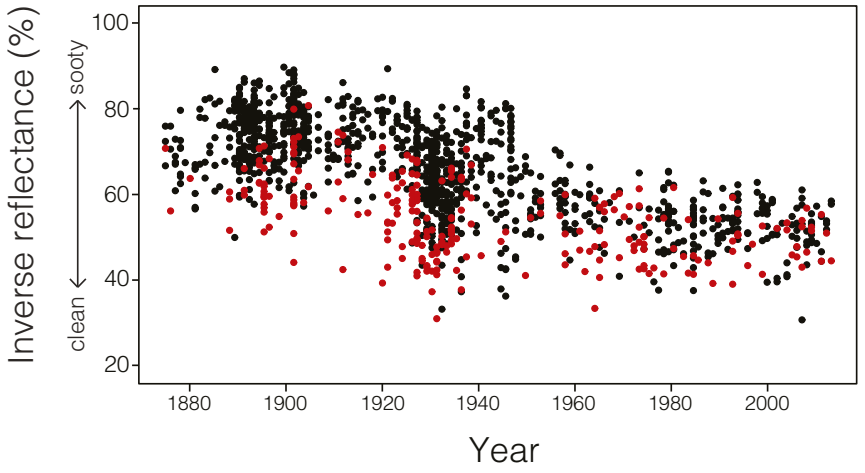

Fig. S5. Black carbon deposition for all 1,347 individuals sampled for this study, showing that specimens from molting months (red points) are substantially cleaner than specimens from winter–summer (black points). Black points are individuals included in the final dataset (n = 1,097), and red points are individuals from molting months that were excluded in final analyses (n = 250) (Fig. S4). Inverse reflectance is reported rather than reflectance to express drops in black carbon emissions, which register as increased reflectance values. Before 1950, individuals from molting months are noticeably cleaner than individuals from the rest of the year, warranting the exclusion of specimens from these months for all years.

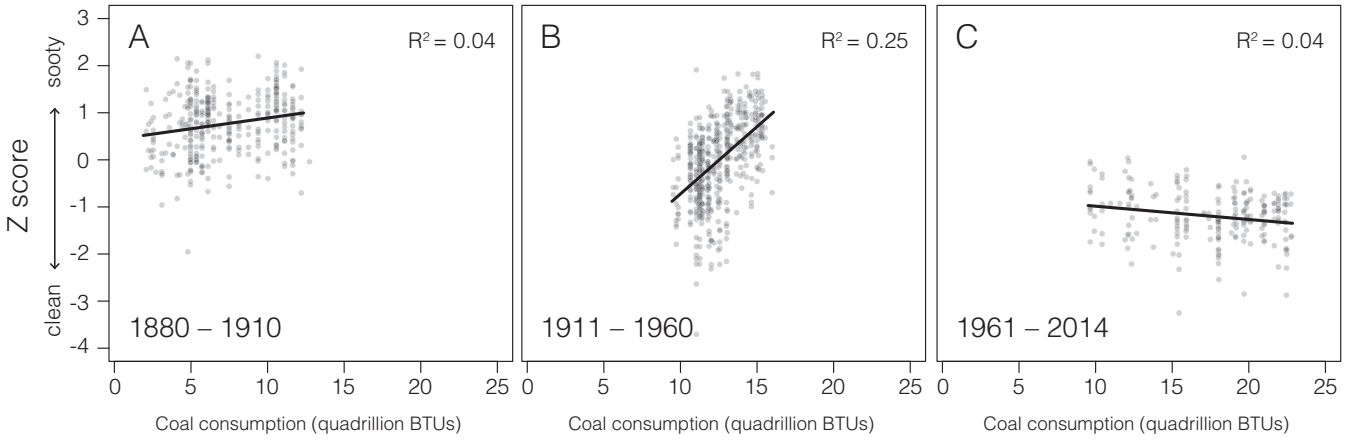

Fig. S6. Black carbon deposition on specimens plotted against US coal consumption for the three time periods defined by the dashed lines in Fig. 2. (*A*) Between 1880 and 1910, black carbon deposition is not correlated with coal consumption. Black carbon deposition is high and remains relatively constant, trending upward only slightly as consumption increases sharply. (*B*) Between 1911 and 1960, black carbon deposition and coal consumption are positively correlated. (*C*) After 1960, black carbon deposition is decoupled from coal consumption. As consumption increases, black carbon deposition remains low. Before 1950, fuel consumption data are only available in 5-y intervals. We thus interpolated consumption values between points to estimate consumption for the year in which each specimen was collected before 1950. After 1950, yearly fuel consumption data are available.

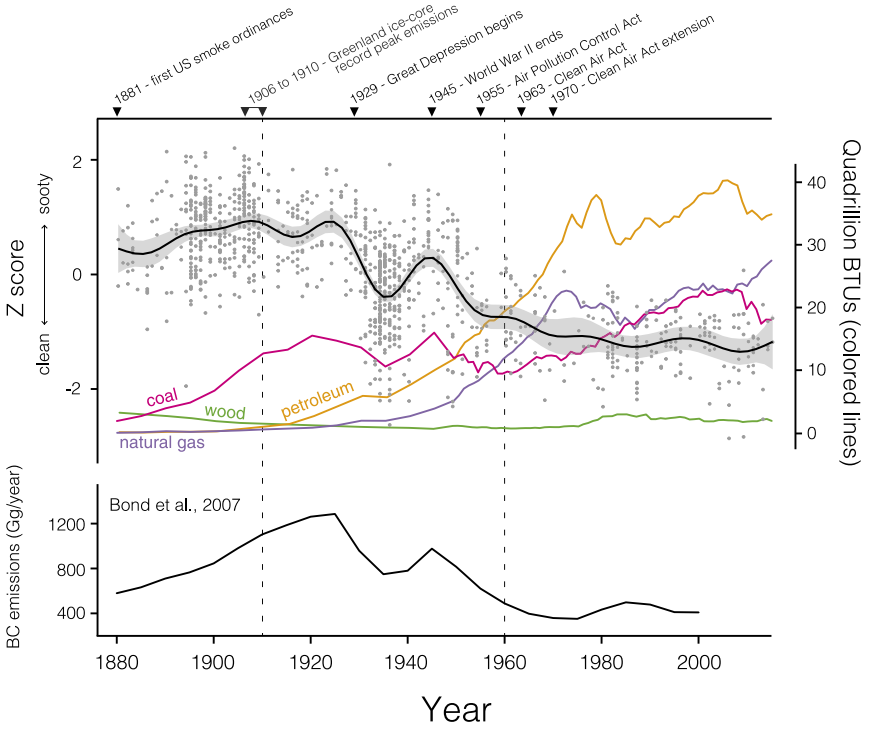

Fig. S7. Black carbon deposition on specimens (five bird species) from the US Manufacturing Belt, collected between 1880 and 2015. Each point represents the z score for an individual specimen (n = 1,097), based on the inverse raw reflectance value taken from its breast and belly feathers. The black line in *Upper* is a GAM (k = 20) with 95% confidence limits (indicated by the shaded area), determined from the individual specimens (details on how k was determined can be found in *SI Materials and Methods* and Fig. S10. Fig. S13 shows species-specific trends). The colored lines are consumption trends for biofuels and fossil fuels expressed in British thermal units (BTUs) (US Energy Information Administration). Before 1950, fuel consumption data are available in 5-y intervals. After 1950, fuel consumption data are yearly. *Lower* shows estimates of total US black carbon (BC) emissions from Bond et al., 2007 (11), which uses fuel consumption data and emission factor data to generate a historical emission inventory. The dashed line at 1910 denotes the progressive shift in cities within the US Manufacturing Belt from prosecuting to educating emissions violators. The dashed line at 1960 denotes the approximate moment after which black carbon emissions becomes decoupled from coal consumption.

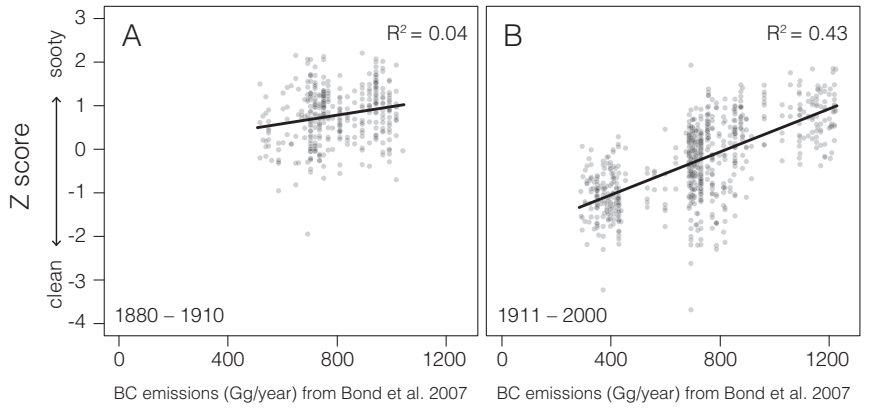

Fig. S8. Black carbon deposition on specimens plotted against black carbon (BC) emissions estimates from Bond et al., 2007 (11) for the three time bins defined in Fig. 2. The second two time bins (1911 to 1960 and 1961 to 2014) are combined to illustrate the strong correlation across both intervals. (*A*) Before 1910, we recovered relatively constant, high levels of black carbon deposition on specimens, while Bond et al., 2007 (11) estimated a sharp rise in black carbon emissions. (*B*) After 1910, black carbon deposition is positively correlated with black carbon emissions estimates from Bond et al., 2007 (11). Our results independently recovered similar trends in atmospheric black carbon. Bond et al., 2007 (11) report BC emissions in 5-y intervals. We thus interpolated emissions values between points to estimate values for the year in which each specimen was collected.

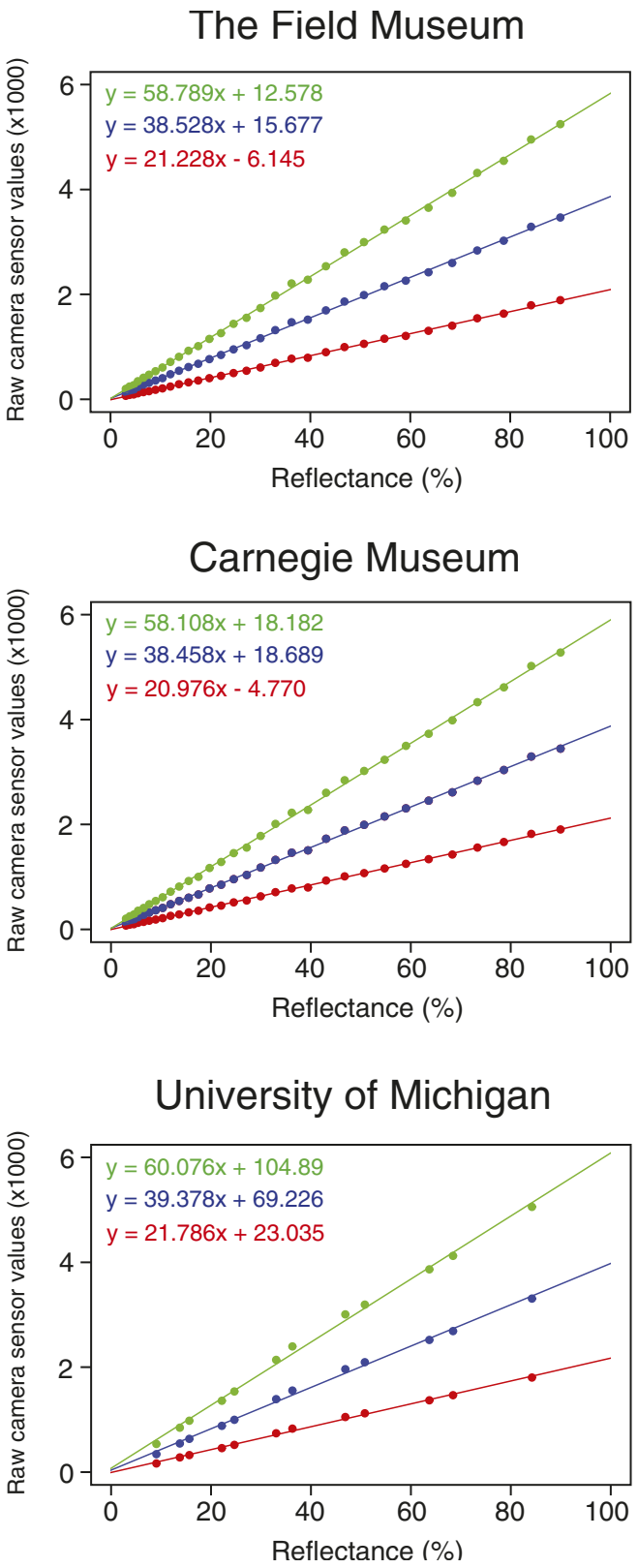

Fig. S9. Raw R, G, and B channel-specific regressions based on the Munsell Neutral Value Scale reflectance standards for each shooting location. The regression equations for each channel were used to calculate channel-specific reflectance from raw CMOS sensor data recovered in RawDigger for each specimen.

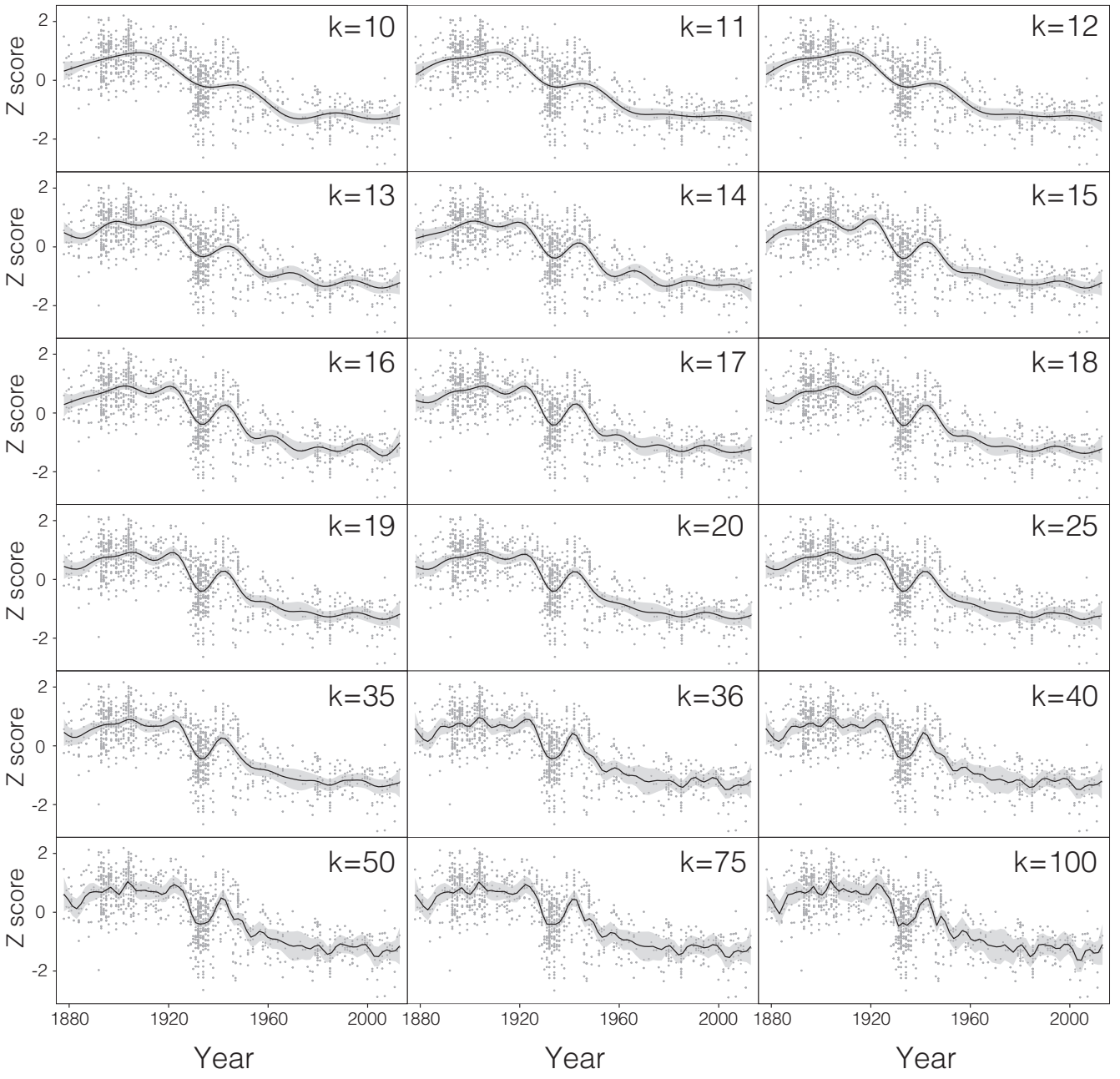

Fig. S10. GAMs with various smoothing functions applied to the normalized 1,097-specimen dataset. k = 10–12 applies an overly powerful smoothing operation in the GAM; k = 13–35 recovers trends that are effectively identical, which appear to recover important signals in the data absent from the k = 10–12 models; and k = 36 (and greater) generates a toothy trend that overrepresents random variations within the sample set.

Fig. S11. Ten Horned Larks (*E. alpestris pratensis*) at The Field Museum, showing that specimens collected in nonindustrial regions do not exhibit comparable levels of soiling to birds collected within the US Manufacturing Belt. The five specimens in *Left* were collected in Illinois, inside the US Manufacturing Belt. The five specimens in *Right* were collected along the western coast of North America, outside of the US Manufacturing Belt. All 10 specimens were collected during nonmolting months (January–April) between 1903 and 1922.

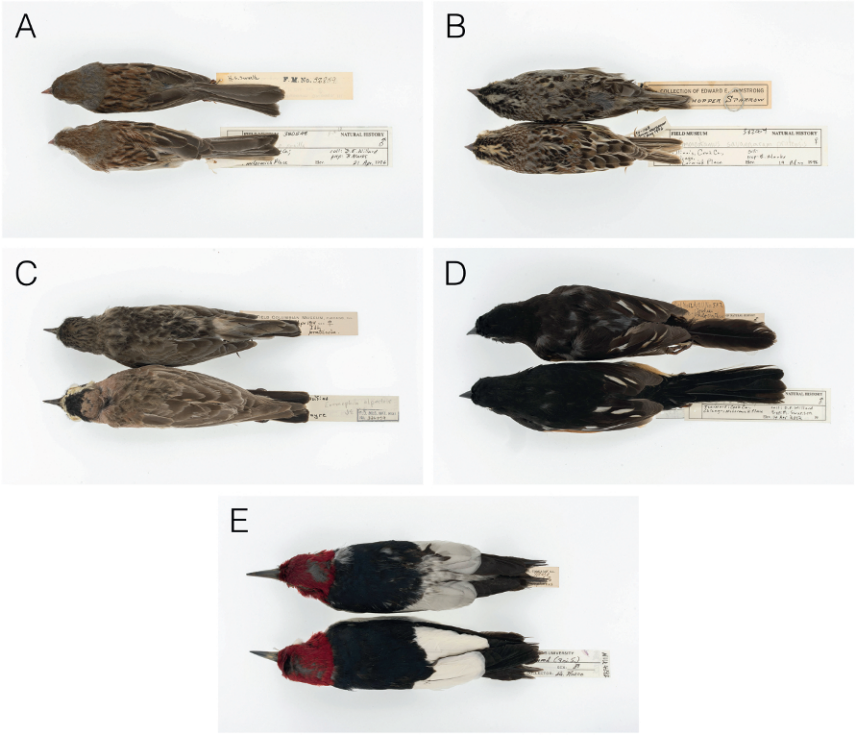

Fig. S12. Images of the dorsal side of specimens from Fig. 1 and Fig. S3. These images, paired with Fig. 1 and Fig. S3, show that even soiling appears over the entire bird, indicating that the soiled birds in our sample acquired black carbon from the environment while alive. (*A*) Field Sparrows (*S. pusilla pusilla*) from 1906 (*Upper*) and 1996 (*Lower*). (*B*) Grasshopper Sparrows (*A. savannarum pratensis*) from 1907 (*Upper*) and 1996 (*Lower*). (*C*) Horned Larks (*E. alpestris pratensis*) from 1904 (*Upper*) and 1966 (*Lower*). (*D*) Eastern Towhees (*P. erythrophthalmus erythrophthalmus*) from 1906 (*Upper*) and 2012 (*Lower*). (*E*) Red-headed Woodpeckers (*M. erythrocephalus*) from 1901 (*Upper*) and 1982 (*Lower*).

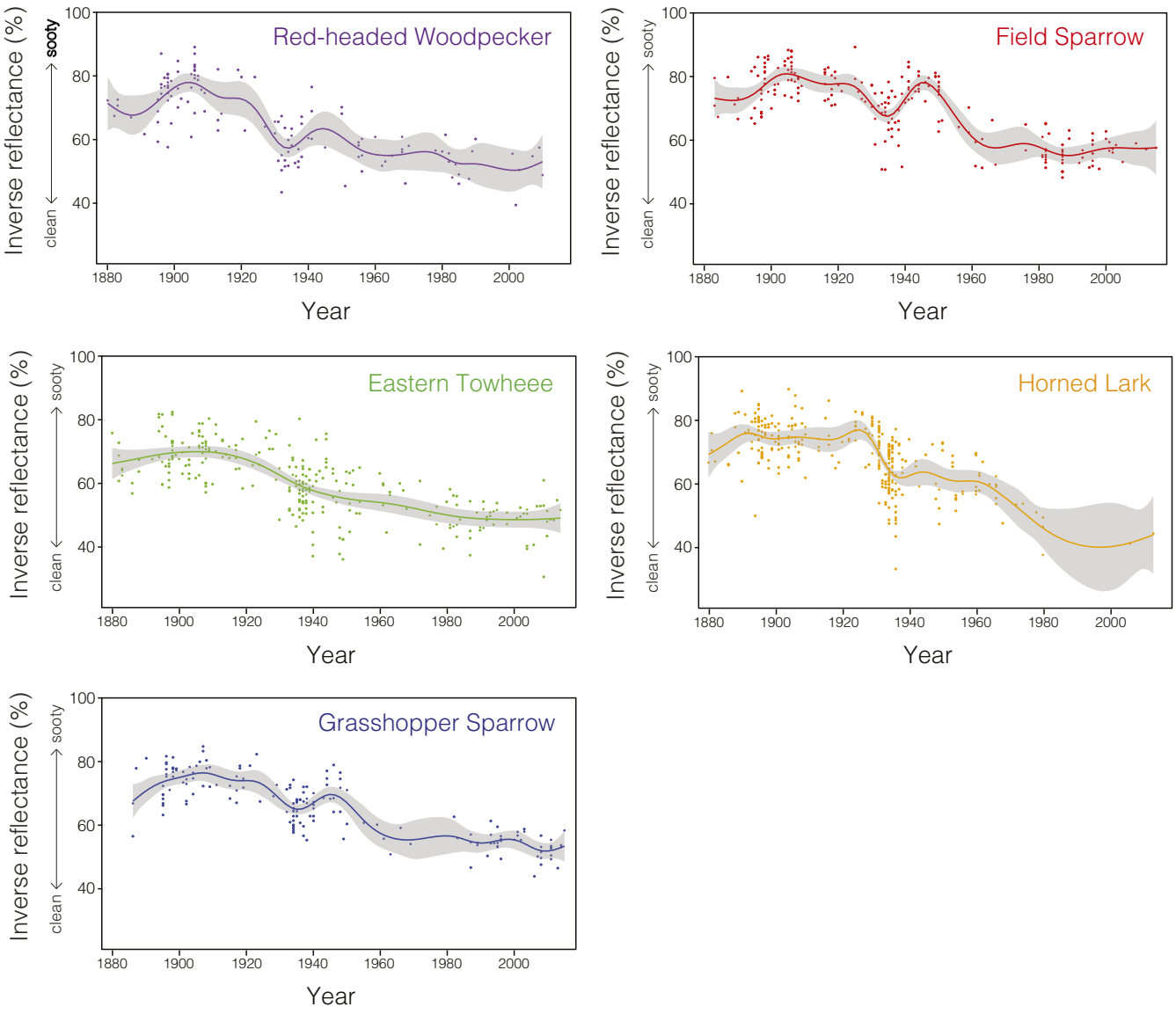

Fig. S13. Species-specific trends in black carbon deposition. Each point represents an individual specimen. The colored lines are GAMs (k = 20) with 95% confidence limits (shaded area) for each species [fall-month birds are excluded (Fig. S4)]. Inverse reflectance is reported, rather than reflectance, to visualize drops in atmospheric black carbon.

Dataset S1. List of vouchered specimens used in the study along with reflectance data

Dataset S1

In Column J, two-letter abbreviations are used for each state. Columns L–O report raw data recorded by the digital camera's CMOS sensor. Column P reports the area sampled on each specimen. Columns Q–T report color channel-specific reflectance values, calculated from the raw sensor data and linear regressions from Fig. S10. CM, Carnegie Museum of Natural History, Pittsburgh; EATO, Eastern Towhee, FISP, Field Sparrow; FMNH, Field Museum of Natural History, Chicago; GHSP, Grasshopper Sparrow; HOLA, Horned Lark; RHWP, Red-headed Woodpecker; UMMZ, University of Michigan Museum of Zoology, Ann Arbor.